NEON IMAGING SPECTROMETER GEOLOCATION PROCESSING ALGORITHM THEORETICAL BASIS DOCUMENT

PREPARED BY	ORGANIZATION	DATE
Thomas Kampe, William Gallery, Tristan Goulden, Nathan Leisso, Keith Krause	AOP	01/07/2013

APPROVALS	ORGANIZATION	APPROVAL DATE
Vlad Aleksiev	PSE	03/01/2016
Andrea Thorpe	SCI	03/01/2016

RELEASED BY	ORGANIZATION	RELEASE DATE
Judy Salazar	CM	03/01/2016

See configuration management system for approval history.

The National Ecological Observatory Network is a project solely funded by the National Science Foundation and managed under cooperative agreement by NEON, Inc. Any opinions, findings, and conclusions or recommendations expressed in this material are those of the author(s) and do not necessarily reflect the views of the National Science Foundation.

Change Record

REVISION	DATE	ECO #	DESCRIPTION OF CHANGE
A	08/25/2014	ECO-01765	Initial release
B	11/20/2015	ECO-02315	Major revision; added Appendix C
C	03/01/2016	ECO-03664	Major Revision; added greater detail to Appendix C mathematics and moved into Section 4.2 – Theory of Algorithm. Changed mathematical notation to be consistent with other AOP documentation.

TABLE OF CONTENTS

LIST OF TABLES AND FIGURES

1 DESCRIPTION

1.1 Purpose

This document details the algorithm used to orthorectify the raw data acquired by the NEON Imaging Spectrometer (NIS). The orthorectification of the NIS data is one of the critical processing steps in deriving the NEON Level-1 data product NEON.DOM.SIT.DP1.30008 Spectrometer Orthorectified at-Sensor Radiance from Level 0 data. The algorithm describes the production orthorectification process for NIS data, the calculation of observation geometry parameters, producing a mosaic of all flight lines collected over a site. The NEON.DOM.SIT.DP1.30008 data product is an intermediate data product in the production of the NEON.DOM.SIT.DP1.30006 L-1 Spectrometer Orthorectified Surface Directional Reflectance data product as described in RD[05]. This document includes a detailed discussion of measurement theory and implementation, appropriate theoretical background, data product provenance, quality assurance and control methods used, approximations and/or assumptions made, and a detailed exposition of uncertainty resulting in a cumulative reported uncertainty for this product.

1.2 Scope

This document describes the theoretical background and algorithmic process for orthorectification of the raw L-0 NEON imaging spectrometer data and co-location with simultaneously acquired LiDAR L-0 data as a necessary step to creating the NEON Level-1 data product NEON.DOM.SIT.DP1.30008 Spectrometer Orthorectified at-Sensor Radiance. It does not provide computational implementation details, except for cases where these stem directly from algorithmic choices explained here.

2 RELATED DOCUMENTS AND ACRONYMS

2.1 Applicable Documents

Applicable documents contain information that shall be applied in the current document. Examples are higher level requirements documents, standards, rules and regulations.

AD[01]	NEON.DOC.000001	NEON Observatory Design
AD[02]	NEON.DOC.005003	NEON Scientific Data Products Catalog
AD[03]	NEON.DOC.005004	NEON Level 1-3 Data Products Catalog
AD[04]	NEON.DOC.005005	NEON Level 0 Data Product Catalog
AD[05]	NEON.DOC.015005	AOP Technical and Operating Requirements
AD[06]	NEON.DOC.015015	AOP Platform Integration Mount Assembly
AD[07]	NEON.DOC.015018	ICD between AOP Payload and Aircraft
AD[08]	NEON.DOC.001292	NEON L0 to L1 Discrete Return Lidar ATBD
AD[09]	NEON.DOC.001211	NEON Digital Camera Orthorectification ATBD
AD[10]	NEON.DOC.000855	AOP Gemini LiDAR System Unit No. 1 Delivery Performance Report

2.2 Reference Documents

Reference documents contain information complementing, explaining, detailing, or otherwise supporting the information included in the current document.

RD[01]	NEON.DOC.000008	NEON Acronym List
RD[02]	NEON.DOC.000243	NEON Glossary of Terms
RD[03]	NEON.DOC.001210	NEON Imaging Spectrometer Calibrated Radiance ATBD
RD[04]	NEON.DOC.001288	NEON Imaging Spectrometer L-1 Radiance to L-1 Reflectance ATBD
RD[05]	NEON.DOC.001289	NEON Imaging Spectrometer Level-1 Processing Overview Document
RD[06]	NEON.DOC.001277	AOP Directory and File Name Conventions

2.3 Acronyms

Acronym	Explanation
ATBD	Algorithm Theoretical Basis Document
IGM	Input Geometry Matrix
GLT	Geometric Lookup Table
ORT	Orthor~~R~~ectified I~~i~~magery Table
OBS	Observation geometry parameter file in pixel-by-pixel format
DP	Data Product
L0	Level 0
L1	Level 1
UQ	Unquantifiable Uncertainty

3 DATA PRODUCT DESCRIPTION

3.1 Variables Reported

The primary outputs from the NEON Imaging Spectrometer (NIS) geolocation algorithm are listed below. Two intermediate data files that are retained for later processing steps are the Input Geometry Files and the Ortho-rectified Geometric Lookup Table file as described in NEON.DOC.001277 AOP Directory and File Name Conventions (RD[06]). These are:

- **Input Geometry File:** Input geometry files (named with "_igm" file extensions) denote the UTM Easting and Northing values derived by the geocorrection process for each original image pixel. If a nominal NIS scene is 598 samples, 1000 lines and 428 bands, then its corresponding input geometry file will be 598 samples, 1000 lines and 2 bands. The first band contains UTM Easting values in meters and the second band contains UTM Northing values in meters for each original pixel. The input geometry files have the same spatial size as the raw NIS imagery. The file is double precision, binary data in a Band Interleaved by Line (BIL) format. The scene elevation, pixel size and UTM zone number information are given in an associated ASCII header file. The input geometry file itself is not orthorectified, but does contain the geolocation information for each original raw pixel.
- **Ortho-corrected geometric lookup table (GLT) files:** Ortho-corrected geometric lookup table files (named with "_glt" file extensions) that contain much of the important information that is created in the geocorrection process. The "_glt" file contains information about which original pixel occupies which output pixel in the final product. Additionally, it is sign-coded to indicate if a certain output pixel is "real" or a nearest-neighbor infill pixel. The "_glt" file is an orthorectified product, with a fixed pixel size projected into a rotated UTM system. The pixel size, scene elevation, UTM zone number and rotation angle information is reported in an associated ASCII header file. The "_glt" file itself is two-byte integer binary data in a BIL format. The two bands of the "_glt" file refer to original sample number and original line number; respectively. The sign of the value indicates whether the pixel is an actual image pixel, located at its proper position (indicated by a positive value) or a nearest-neighbor infill pixel placed to fill an undersampling image gap (indicated by a negative value). The geometric lookup table image, along with the raw imagery, can be used to geocorrect any band or derived product through a simple lookup table procedure. A sample GLT image is shown in Figure 1.

Two data files are produced as the final output of the geolocation processing. The first of these are used to produce the L-1 Ortho-rectified spectral radiance data Product.

- **OrthoRectified imagery Table (ORT) files:** Orthorectified imagery Table files are produced by applying the geometric lookup tables to the entire NIS data set (i.e., all spectral bands) to create a fully orthorectified image cube. These files (named with "__geo" extensions) represent the final imaging spectrometer orthorectified radiances at the flight line level.

- **Mosaic multi-file mosaic (MOS_ORT) orthorectified files:** the MOS_ORT files are mosaics of **multiple** flight lines of the orthorectified radiances stored as a single file.

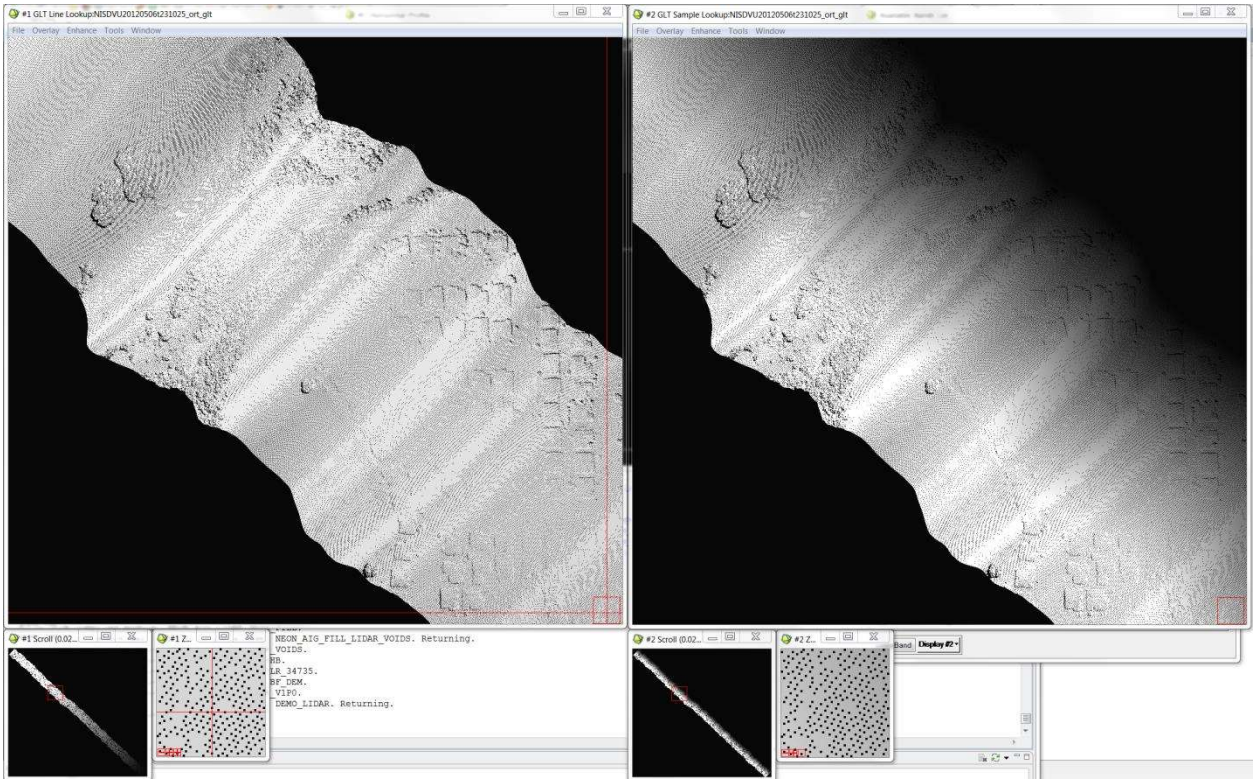

Figure 1. Sample GLT Image. The GLT files contain information about which original pixel occupies which output pixel in the final product. The GLT output is sign-coded to indicate whether a certain pixel contains real data (positive) or if it is nearest-neighbor infill pixel (negative).

3.2 Input Dependencies

There are several necessary inputs required to support the geolocation processing of the NEON imaging spectrometer data. These are provided from the LiDAR processing and external data sources. These inputs are described in the following paragraphs and represented in the processing flow diagram in Figure 2.

- **Earth Gravitational Model 1996 (EGM96) EGM96 Geoid file:** An individual file is created for each region flown. An improved spherical harmonic model of the Earth's gravitational potential to degree 360 developed by the NASA Goddard Space Flight Center (GSFC), the National Imagery and Mapping Agency (NIMA), and the Ohio State University (OSU). The new model, Earth Gravitational Model 1996 incorporates improved surface gravity data, altimeter-derived anomalies from ERS-1 and from the GEOSAT Geodetic Mission (GM), extensive satellite tracking

data - including new data from Satellite laser ranging (SLR), the Global Positioning System (GPS), NASA's Tracking and Data Relay Satellite System (TDRSS), the French DORIS system, and the US Navy TRANET Doppler tracking system - as well as direct altimeter ranges from TOPEX/POSEIDON (T/P), ERS-1, and GEOSAT. The final solution blends a low-degree combination model to degree 70, a block-diagonal solution from degree 71 to 359, and a quadrature solution at degree 360. The model was used to compute geoid undulations accurate to better than one meter (with the exception of areas void of dense and accurate surface gravity data) and provide WGS84 as a true three-dimensional reference system (http://cddis.nasa.gov/926/egm96/nasatm.html).

- **SBET (smoothed best estimate trajectory) file:** this file is a product of the LiDAR geolocation processing.
- **Processed radiance file:** this is the spectrometer spectral radiance data, as processed through the NIS calibration algorithm (RD [03]).
- **Merged Digital Elevation Map (DEM) for region of interest:** a DEM is generated during the LiDAR geolocation processing but this may have gaps in coverage (between flight lines, etc.). For this reason the LiDAR-generated DEM is merged with an externally-generated DEM (typically, a USGS product) to create the merged DEM providing full spatial coverage of the region of interest. The merged DEM is a product of the LiDAR processing.
- **NIS Camera Model:** this model provides as input the distortion introduced by the imaging spectrometer into the retrieved data and the measured lever arms between the NIS focal plane and the LiDAR scan mirror. These parameters are unique to each NIS instrument and in the case of the lever arms, unique to each installation of the NIS into the aircraft. The NIS distortion, characterized by the measured curvature of the projected focal plane, is provided as part of the instrument calibration file by the instrument vendor, NASA JPL. This information is coded into the unique camera file for each instrument one time. As stated previously, the NIS focal plane-to-LiDAR mirror lever arms must be measured for each installation in to the aircraft and are manually entered in the neon_aig_vswir_ortho_apply_lever_arm.pro subroutine prior to processing.

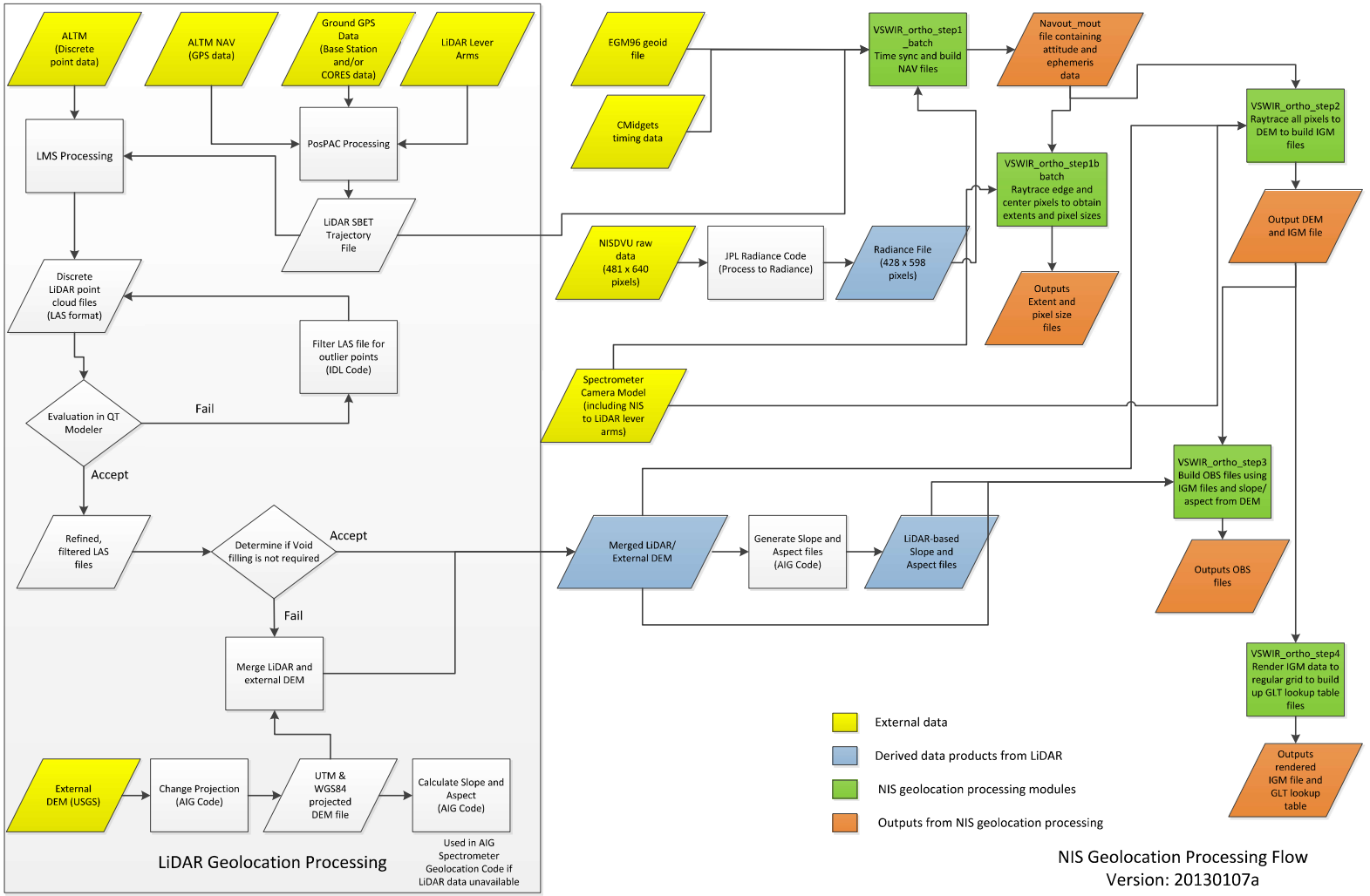

Figure 2. NIS geolocation processing flow

3.3 Product Instances

The NEON.DOM.SIT.DP1.30008 L-1 Spectrometer Orthorectified at-Sensor Radiance L-1 Data Product is a product of this algorithm.

3.4 Temporal Resolution and Extent

The NIS geolocation algorithm is applied on each AOP flight line, which typically measure between 5 and 20 km in length and approximately 600 m in width. Typical flight altitudes are approximately 1000m Above Ground Level (AGL). Flight speeds are generally around 100 knots (185.2 km/hour), and therefore, the time required to acquire flight lines of the lengths stated will range from 1.6 to 6.5 minutes. The integration time for the NIS detector array is 100 milliseconds, so an image is acquired every 100 milliseconds along-track.

3.5 Spatial Resolution and Extent

The NIS geolocation algorithm is applied on each AOP flight line, which typically measure between 5 and 20 km in length and approximately 600 m in width. The Instantaneous Field of View (IFOV) of the NEON Imaging Spectrometer is 1.0 milliradian, which equates to a ground sampling distance (GSD) of 1 meter at a nominal flight of 1000 m above ground. The actual ground resolution will vary with flight altitude and cross-track field angle.

4 SCIENTIFIC CONTEXT

A critical first step in the processing of imaging spectrometer data is the accurate orthorectification of the raw data to eliminate the distortion introduced by aircraft motion and atmospheric turbulence. In addition, in this process the spectrometer data is co-registered to the LiDAR data that is acquired simultaneously from the NEON Airborne Observation Platform (AOP). The outputs from this processing are accurate projections of each individual imaging spectrometer pixel onto a map grid and the precise geometric coordinates for each pixel. The high precision and high accuracy trajectory and attitude information obtained from the onboard GPS/INS system form the common link for the detailed ray tracing of the NEON imaging spectrometer, LiDAR , and subsequently, the digital camera. These sensors all receive the same GPS time stamping from the imaging spectrometer IMU, which allows for the common use of the GPS-IMU data between instruments. The LiDAR GPS and Inertial Measurement Unit (IMU) accelerometers provide the precise information on aircraft position and attitude; respectively. Measurements of the lever-arms (or offsets) between the GPS antenna, IMU, LiDAR, and imaging spectrometer optical centers and subsequent optimization in the optical models of the two sensor heads provide the precise co-location and projected geo-location of all data in post-flight processing.

4.1 Theory of Measurement/Observation

The remote sensing payload being flown onboard NEON's Airborne Observation Platform (AOP) includes the NEON Imaging Spectrometer (NIS), a visible-to-shortwave infrared (VSWIR) pushbroom imaging spectrometer (NIS); a small-footprint full waveform LiDAR, and a high-resolution digital camera (AD[05]). The instrument payload is mounted onto a common integration plate, the Platform Integration Mount, or PIM (AD[06]). The entire AOP remote sensing payload is integrated onto a de Havilland DHC-6 Twin Otter aircraft configured with a large open downward-looking viewing port. The payload is mounted directly on the cabin floor via the seat rails with the sensors viewing in the nadir direction through the open port (AD[07]).

Since the payload is mounted directly to the airframe, there is no active roll compensation during flight. Any aircraft motion or vibration will result in image distortion. The raw imagery acquired with the NIS and LiDAR is usually distorted by turbulence and aircraft roll, pitch, and yaw (Figure 3). Following the orthorectification and co-location process described in this document, ortho-rectification of the spectrometer data is achieved referenced to a uniform grid defined by the LiDAR data as shown in Figure 4. Through this process, the imaging spectrometer data is also co-registered to data retrieved by the LiDAR. Co-registration between the two instruments is particularly challenging due to the different scanning geometries employed by the two sensors (Appendix 1. Scanning Geometries of the LiDAR and NIS).

For this reason, a necessary first step in the L-0 to L-1 imaging spectrometer data processing chain is the precision orthorectification of the LiDAR discrete return ranges. This aspect of the processing chain is described in the NEON L0 to L1 Discrete Return LiDAR Algorithm Theoretical Basis Document (AD[08]).

The Optech Gemini LiDAR is provided with a high accuracy Applanix Inertial Measurement Unit (IMU) and GPS system. The positional information from the GPS and the 3-axis attitude data from the IMU accelerometers are combined in a tightly coupled Kalman filter approach to give real-time information on the x, y, and z position as well as roll, pitch, and true heading of the sensors on board the aircraft. The IMU that is installed on the platform integration mount as part of the NIS system is used exclusively to provide a timestamp for acquired data frames from the imaging spectrometer.

Figure 3. Sample raw imaging spectrometer radiance image

Figure 4. Sample Orthorectified NEON Imaging Spectrometer Radiance Image

In the imaging spectrometer geolocation procedure, each pixel is individually raytraced from the airborne platform to the ground using a full optical sensor model and trajectory data. The geolocation of the LiDAR data is conducted prior to processing of the imaging spectrometer data and a digital elevation map (DEM) is generated from the LiDAR first returns. This process is described in AD[07]. The pixels at the focal plane of the imaging spectrometer are then ray traced to the surface defined by the DEM generated from the DEM data.

The general method employed in the orthorectification of the imaging spectrometer data and co-registration to the LiDAR data is the use of the standard Euler Angle (Figure 5) approach to rotate the NIS principal plane according to the roll, pitch, and true heading of the aircraft that is recorded by the Applanix IMU integral to the LiDAR system. By accounting for aircraft velocity, the timing of focal plane image acquisition, lever arms between the LiDAR and imaging spectrometer, and incorporating an accurate camera model for the spectrometer, a position and pointing vector is calculated for each NIS image pixel. Best estimates of each imaging spectrometer pixel location center with respect to the geodesic coordinates defined by the LiDAR DEM in three dimensions are made to produce co-located and orthorectified maps of the imaging spectrometer and LiDAR data that are reported on the Universal Transverse Mercator (UTM) projection system. The precision locational information for each imaging spectrometer pixel is then available for detailed spectroscopic modeling and is used in subsequent processing for rendering the LiDAR and imaging spectrometer data sets onto a common grid for overlay, comparison, and product generation. A similar processing methodology is employed to orthorectify the digital camera imagery to the common grid defined by the LiDAR -generated DEM (AD[09]).

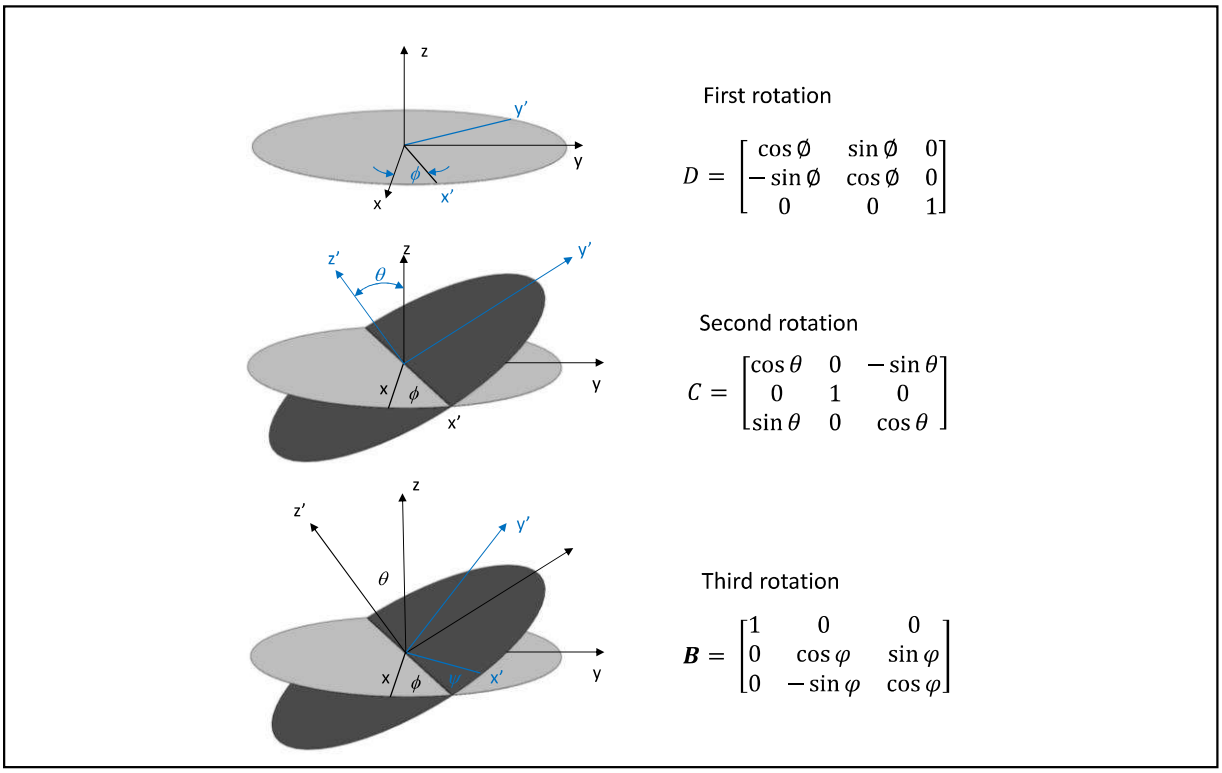

Figure 5. Euler Angles

4.2 Theory of Algorithm

The georeferencing of the airborne imaging spectrometer data is a problem of transforming the 3-D vector (u_s) of a pixel sensor in the spectrometer sensor frame (*s*-frame) to the 3-D vector (u_m) of the pixel in the UTM mapping frame for any given instant of time an observation is acquired and then ray-tracing the vector until an intersection with the earth's surface occurs. The transformation between the spectrometer sensor reference frame (s-frame) and the mapping frame of the earth surface (m-frame) is illustrated in Figure 6, and details can also be found in El-Sheimy (2009).

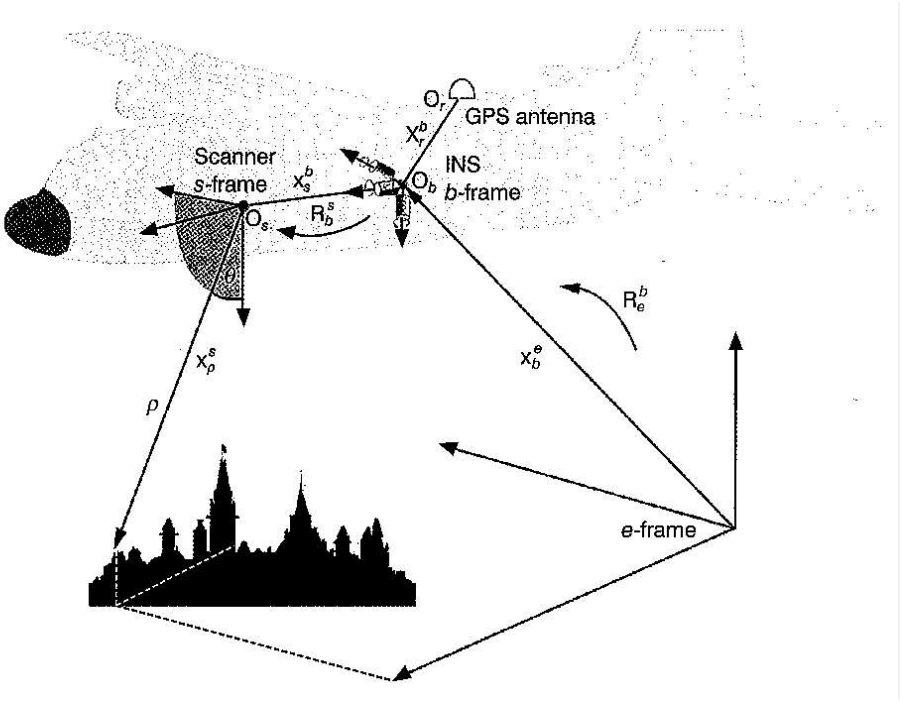

Figure 6 - Coordinate Transformation from Sensor Frame to Surface Frame

The sensor reference frame (*s*-frame), has a positive *x*-direction parallel to the direction of flight, positive *y*-axis along the sensor axis length and positive z-axis direction downward and origin at the perspective center of the sensor. Note that since the NIS is a push-broom type sensor, the *x*-component in the sensor frame will always be zero. The *s*-frame will change position and orientation with respect to the mapping reference frame *(m*-frame) with time as a result of aircraft velocity, elevation, and orientation. Geo-referencing and ray-tracing is possible at any instant of time if the sensor position in the *m*-frame (v_m) and the appropriate intermediate rotations and translations between the *s*-frame and the *m*-frame, are known. The first step in achieving u_m is the transfer of u_s to the body frame (*b*-frame) by rotating by the boresight angles follows:

$$\boldsymbol{u}_b = \mathbf{R}_s^b u_s \tag{1}$$

where

$$\mathbf{R}_s^b = \mathbf{R}_{\beta_x}\mathbf{R}_{\beta_y}\mathbf{R}_{\beta_z} = \begin{bmatrix} 1 & 0 & 0 \\ 0 & \cos\beta_x & \sin\beta_x \\ 0 & -\sin\beta_x & \cos\beta_x \end{bmatrix} \begin{bmatrix} \cos\beta_y & 0 & -\sin\beta_y \\ 0 & 1 & 0 \\ \sin\beta_y & 0 & \cos\beta_y \end{bmatrix} \begin{bmatrix} \cos\beta_z & \sin\beta_z & 0 \\ -\sin\beta_z & \cos\beta_z & 0 \\ 0 & 0 & 1 \end{bmatrix} \tag{2}$$

and β_x, β_y, and β_z are the boresight angular rotations about the *x*-axis, *y*-axis and *z*-axis of the *s*-frame respectively. The rotation matrices in eq. 2 can be combined and written as

$$\mathbf{R}_s^b = \begin{bmatrix} \cos\beta_x\cos\beta_z & \cos\beta_y\sin\beta_z & -\sin\beta_y \\ \sin\beta_x\sin\beta_y\cos\beta_z - \cos\beta_x\sin\beta_z & \sin\beta_x\sin\beta_y\sin\beta_z + \cos\beta_x\cos\beta_z & \sin\beta_x\cos\beta_y \\ \cos\beta_x\sin\beta_y\cos\beta_z + \sin\beta_x\sin\beta_z & \cos\beta_x\sin\beta_y\sin\beta_z - \sin\beta_x\cos\beta_z & \cos\beta_x\cos\beta_y \end{bmatrix}. \quad (3)$$

The orientation of the *b*-frame is an important consideration during the transfer of $\boldsymbol{u_s}$ to $\boldsymbol{u_b}$ as the sign on each $\beta_{x,y,z}$ is critical. Since the *s*-frame is a right-handed system, boresight angles with positive sign will initiate clockwise rotations when looking down the positive direction of each respective axis. Therefore, when determining the boresight angles from the in-flight calibration procedure, care must be taken to ensure the rotations are produced with the appropriate sign. It should also be noted that boresight angles are typically small, often only fractions of a degree. Under these conditions, we can use the approximates $cos(\beta) \approx 1$ and $sin(\beta) \approx \beta$, which allow a simplification of Eq. 3 to

$$\boldsymbol{R}_s^b = \begin{bmatrix} 1 & \beta_z & -\beta_y \\ -\beta_z & 1 & \beta_x \\ \beta_y & \beta_x & 1 \end{bmatrix} \quad (4)$$

Once in the body frame, $\boldsymbol{u_b}$ can be transferred to the navigation frame (*n*). The *n*-frame has positive *x*-direction toward geodetic north (true north), *y*-axis with positive direction toward east and *z*-axis with positive direction toward the local ellipsoidal normal (Figure 7). This frame is also commonly referred to as a *NED* (north-east-down) geographic frame (see Abdullah et al., 2013). The transfer of $\boldsymbol{u_b}$ to the *n*-frame requires the roll (φ), pitch (θ) and yaw (ψ) values as observed by the IMU. Similar to the boresight angles, the sign of these measurements as recorded by the IMU is an important consideration. According to the definition of the *b*-frame described by Applanix (2012), positive angular changes will result in roll when the aircraft's right wing tips down, in pitch when the aircraft's nose tips up, and in heading when the aircraft makes a right-hand turn. To transfer $\boldsymbol{u_b}$ from the *n*-frame to the *b*-frame, a similar relationship as shown in (3) and (4) can be used, with values for roll, pitch and yaw substituted for the boresight angles. This combination follows the traditional aerospace sequence (Kuipers, 1999) of Euler angle rotations (Figure 5), and can be written as

$$\mathbf{R}_n^b = \mathbf{R}_\varphi\mathbf{R}_\theta\mathbf{R}_\psi = \begin{bmatrix} 1 & 0 & 0 \\ 0 & \cos\varphi & \sin\varphi \\ 0 & -\sin\varphi & \cos\varphi \end{bmatrix}\begin{bmatrix} \cos\theta & 0 & -\sin\theta \\ 0 & 1 & 0 \\ \sin\theta & 0 & \cos\theta \end{bmatrix}\begin{bmatrix} \cos\psi & \sin\psi & 0 \\ -\sin\psi & \cos\psi & 0 \\ 0 & 0 & 1 \end{bmatrix} \quad (5)$$

which can be combined to

$$\mathbf{R}_n^b = \begin{bmatrix} \cos\varphi\cos\psi & \cos\theta\sin\psi & -\sin\theta \\ \sin\varphi\sin\theta\cos\psi - \cos\varphi\sin\psi & \sin\varphi\sin\theta\sin\psi + \cos\varphi\cos\psi & \sin\varphi\cos\theta \\ \cos\varphi\sin\theta\cos\psi + \sin\varphi\sin\psi & \cos\varphi\sin\theta\sin\psi - \sin\varphi\cos\psi & \cos\varphi\cos\theta \end{bmatrix}. \quad (6)$$

However, note that this provides a rotation from the *n*-frame to the *b*-frame, where we desire the rotation from the *b*-frame to the *n*-frame, i.e. the inverse rotation is required. Since rotation matrices of Euler angles are orthogonal, the combined rotation matrix is also orthogonal, and for any orthogonal matrix it holds true that

$$\mathbf{R}^T = \mathbf{R}^{-1} \quad (7)$$

from which it follows that (Jekili, 2000, pg. 11)

$$\left(\mathbf{R}_\varphi \mathbf{R}_\theta \mathbf{R}_\psi\right)^{-1} = \left(\mathbf{R}_\varphi \mathbf{R}_\theta \mathbf{R}_\psi\right)^T. \quad (8)$$

This relationship can be exploited to achieve the inverse rotation of $\mathbf{R}_n^b$ by applying the transpose operation; therefore

$$\mathbf{R}_b^n = [\mathbf{R}_n^b]^{\mathrm{T}} \begin{bmatrix} \cos\varphi\cos\psi & \sin\varphi\sin\theta\cos\psi - \cos\varphi\sin\psi & \cos\varphi\sin\theta\cos\psi + \sin\varphi\sin\psi \\ \cos\theta\sin\psi & \sin\varphi\sin\theta\sin\psi + \cos\varphi\cos\psi & \cos\varphi\sin\theta\sin\psi - \sin\varphi\cos\psi \\ -\sin\theta & \sin\varphi\cos\theta & \cos\varphi\cos\theta \end{bmatrix}. \quad (9)$$

and it follows that

$$\boldsymbol{u}_n = \mathbf{R}_b^n u_b. \quad (10)$$

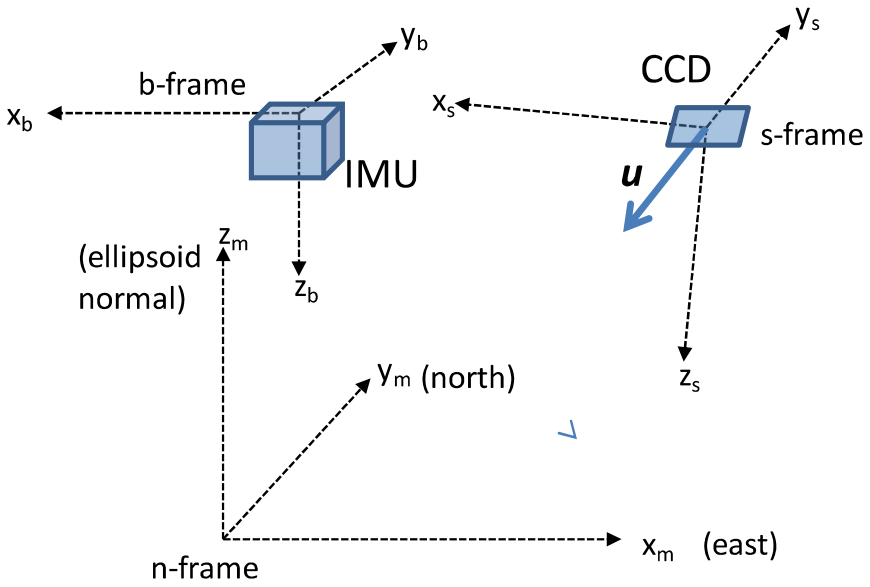

Figure 7 - Relationship between the *s*-frame, *b*-frame and *n*-frame

Ultimately, we desire $\boldsymbol{u}$ to be in a global reference frame, as opposed to the local *n*-frame. To convert to a global mapping frame, we first determine $\boldsymbol{u}_n$ in an ECEF (Earth centered earth fixed) frame. The ECEF frame is a Cartesian frame with origin at the center of a reference ellipsoid, positive direction of the *x*-axis toward the intersection of the equator and Greenwich meridian, *y*-axis with positive direction toward the intersection of the equator and 90° east meridian, and *z*-axis with positive direction through the geographic north-pole. The transfer of $\boldsymbol{u_n}$ to ECEF coordinates is performed as follows

$$\boldsymbol{u}_{ECEF} = \mathbf{R}_n^{ECEF} u_n \tag{11}$$

where, following Jekeli (2000, pg. 25),

$$\begin{aligned}\mathbf{R}_n^{ECEF} &= \begin{bmatrix}\cos(-\lambda) & 0 & -\sin(-\lambda)\\ 0 & 1 & 0\\ \sin(-\lambda) & 0 & \cos(-\lambda)\end{bmatrix}\begin{bmatrix}\cos(\pi/2+\phi) & \sin(\pi/2+\phi) & 0\\ -\sin(\pi/2+\phi) & \cos(\pi/2+\phi) & 0\\ 0 & 0 & 1\end{bmatrix}\\ &= \begin{bmatrix}-\sin\phi\cos\lambda & -\sin\lambda & -\cos\phi\cos\lambda\\ -\sin\phi\sin\lambda & \cos\lambda & -\cos\phi\sin\lambda\\ \cos\phi & 0 & -\sin\phi\end{bmatrix}.\end{aligned} \tag{12}$$

where ϕ and λ are the latitude and longitude of the principal point sensors perspective center. At this stage, $\boldsymbol{u}_{ECEF}$ is has origin at the sensor focal point, however, the absolute location of the aircraft given by the SBET is at a reference point on the IMU. The coordinates must be transferred from the IMU

reference point to the sensor focal point (*O*). Let the location of *O* be described with $\boldsymbol{v}$**.** The translation distances between these two locations is physically measured in the lab and are termed the 'lever arms' (Figure 8, Figure 9). The determination of the location of the sensor focal point in the *ECEF* frame is performed as follows:

$$\boldsymbol{v}_{ECEF} = \mathbf{R}_n^{ECEF}\mathbf{R}_b^n\left(\boldsymbol{l}_b + \boldsymbol{R}_{\boldsymbol{n}}^{\boldsymbol{b}}\boldsymbol{R}_{\boldsymbol{ECEF}}^{\boldsymbol{n}}\boldsymbol{s}_{ECEF}\right) \tag{13}$$

where $\boldsymbol{s}$ is the location of aircraft at the IMU reference point, and $\boldsymbol{l}$ is the measured lever arm offsets (Figure 8, Figure 9). The *ECEF* coordinates can be translated into latitude and longitude to put $\boldsymbol{v}_{ECEF}$ into a geographic frame (*G*) using well known relationships (Jekeli, 2001, pg.24), as follows

$$v_G = \begin{bmatrix}\phi\\ \lambda\\ h\end{bmatrix}_G = \begin{bmatrix}\tan^{-1}\left(\dfrac{z_{ECEF}}{\sqrt{{x_{ECEF}}^2 + {y_{ECEF}}^2}}\left(1 + \dfrac{e^2 N \sin\phi}{z_{ECEF}}\right)\right)\\ \tan^{-1}\left(\dfrac{y_{ECEF}}{x_{ECEF}}\right)\\ \dfrac{\sqrt{{x_{ECEF}}^2 + {y_{ECEF}}^2}}{\cos\phi} - N\end{bmatrix} \tag{14}$$

where *h* is the ellipsoidal height measured along the ellipsoidal normal, *N* is the radius of curvature of the reference ellipsoid in the prime vertical plane, determined as

$$N = \frac{a}{\sqrt{1 - e^2\sin^2\phi}} \tag{15}$$

where *a* is the semi-major axis of the reference ellipsoid, and e is the eccentricity which is determined as

$$e^2 = 2f - f^2 \tag{16}$$

and *f* is the flattening for the specific desired reference ellipsoid. For reference, the values for the semi-major axis and flattening of the GRS80 ellipsoid, which is used in the WGS84 datum, are 6378137 m and 1/298.257222101 respectively. The solution for ϕ in (14) is not a closed form solution, and an iterative procedure must be employed to achieve a result of sufficient accuracy. This requires an initial estimate of ϕ, where *h* is assumed to be zero, determined as follows

$$\phi_0 \equiv \phi(h=0) = \tan^{-1}\left(\frac{z_{ECEF}}{\sqrt{x_{ECEF}^{\ 2} + y_{ECEF}^{\ 2}}}\left(\frac{1}{1-e^2}\right)\right) \tag{17}$$

and through each successive iteration, (15) and (16) must be updated. Once $\boldsymbol{v}_G$ and $\boldsymbol{u}_G$ are in geographic coordinates, they can be converted to UTM coordinates for ray-tracing $\boldsymbol{u}$ to a DSM (also in the UTM mapping frame). To convert geographic coordinates to UTM coordinates well-known formulations from Snyder (1989) can be implemented, and these are not necessarily repeated here. The direction indicated by $\boldsymbol{u}_{ECEF}$ can be applied to $\boldsymbol{v}_{ECEF}$ to provide the direction of the LOS in the ECEF frame. If the vector is extended, the end point can be transformed to UTM coordinates with equations 19 through 22. Once the vector is established in the UTM mapping frame, it can be ray-traced onto a DTM (also in the UTM mapping projection) to determine pixel location on the ground.

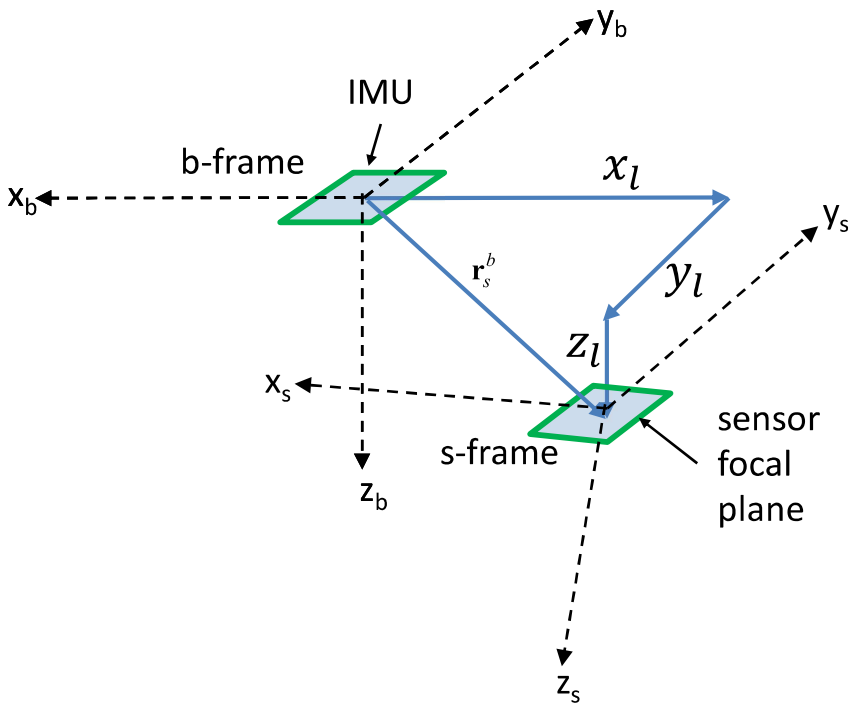

Figure 8 - Translational relationship between the *b*-frame and the *s*-frame through the three components of the lever arm vector between the IMU and the sensor focal plane.

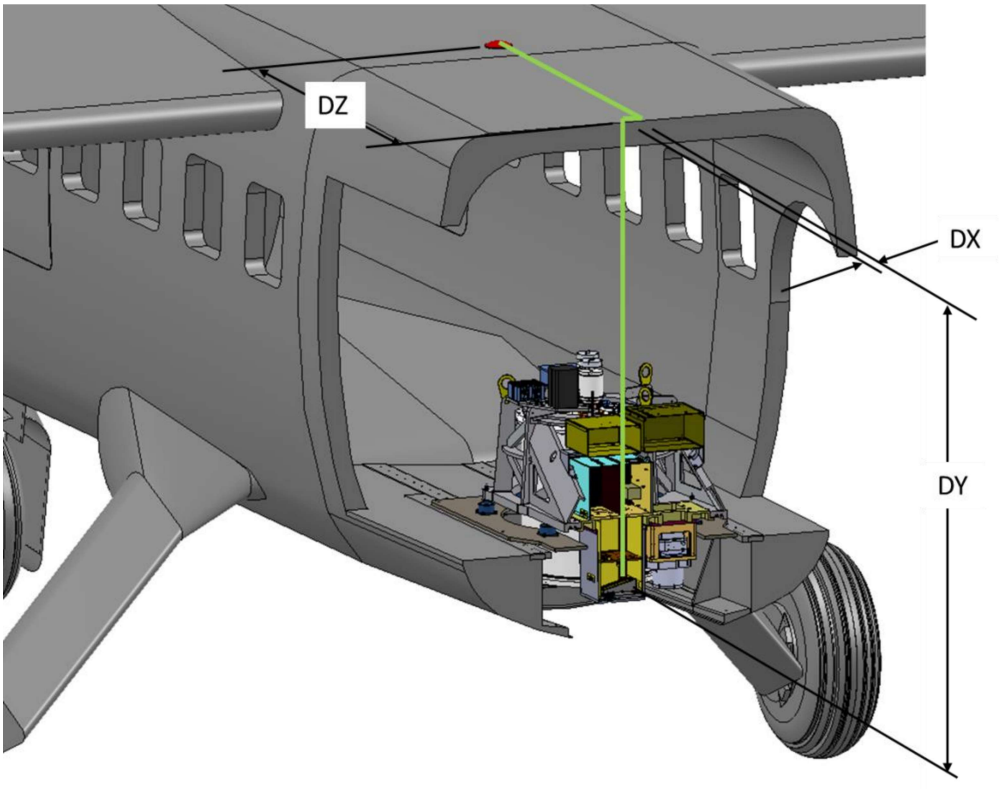

Figure 9 - Lever arm calculations for the NISDVU for the configuration flown during May 2012

5 ALGORITHM IMPLEMENTATION

5.1 Production Processing Flow

The processing of the raw imaging spectrometer data to the final orthorectified data is achieved in the following steps. These are also represented in the processing flow diagram of Figure 2. A list of the ~~the~~ files involved in the processing is included as Appendix B: List of Files.

The imaging spectrometer geolocation algorithm has been implemented in IDL and calls several ENVI functions.

Step 1: Initial processing of the raw data. This step performs the time sync between the imaging spectrometer image frames and navigation data as provided from the LiDAR geolocation processing.

- Inputs: image and sbet files:
  - egm96 geoid file, the desired down track binning factor, a flag to tell it if the raw files are only three bands or full 481-band data, the UTM time zone and file names of the raw image file, the processed radiance file that indicates the starting raw sample and frame, and the sbet navigation file

- Output: ephemeris and attitude files as well as timing files that contain the data needed to ray trace from the pixels on the ground to the imaging spectrometer image plane:
    - Navout_mout : navigation parameter output file containing attitude and ephemeris data for orthorectification.

Step 1b: Conducts a quick ray tracing of the three center pixels and the two edge pixels to find the extent of the corrected images and to gather statistics on the mean down-track and cross-track pixel spacings. Output from a sample Step 1b report file is shown in Table 1.

- Inputs:
  - name of report file to create
  - a mode flag to ray trace only the 5 pixels per line
  - a flag to indicate if ENVI is available
  - the UTM zone, the DEM file to use
  - the names of the navout_mout files created in Step 1
  - the name of the camera file (a unique camera file is generated for each imaging spectrometer)
  - bin factor being used
- Output:
  - Output report

Table 1. Sample Step 1b Report File. The parameters being reported are the minimum and maximum extents of the imaged camera pixels on the ground (in meters) and the down-track pixel spacings (dt_ps) and cross-track pixel spacings (at_ps) in pixel units.

Tue May 08 23:30:37 2012						
neon step1b report file						
file, xmin, xmax, ymin, ymax, dt_ps, at_ps						
G:\gj0512\20120505\NISDVU20120505t171541	716598.548	721321.618	4326770.690	4330128.230	0.974	3.423
G:\gj0512\20120505\NISDVU20120505t175337	713966.592	718783.890	4326936.518	4331747.816	0.509	1.188
G:\gj0512\20120505\NISDVU20120505t180354	714386.039	719319.931	4328043.058	4332788.129	0.667	1.143
G:\gj0512\20120505\NISDVU20120505t181309	713268.245	718189.197	4327397.653	4332319.707	0.727	1.170
G:\gj0512\20120505\NISDVU20120505t182046	714711.815	719185.100	4327506.004	4331716.742	0.748	1.200
G:\gj0512\20120505\NISDVU20120505t183058	714343.934	718867.336	4328338.821	4332800.522	0.642	1.195
G:\gj0512\20120505\NISDVU20120505t183826	715407.425	719635.856	4328304.897	4332293.735	0.674	1.146
G:\gj0512\20120505\NISDVU20120505t184822	716174.793	717739.346	4327195.717	4333793.142	0.690	1.172
G:\gj0512\20120505\NISDVU20120505t185341	723598.910	725074.293	4330342.646	4337627.588	0.759	1.215
G:\gj0512\20120505\NISDVU20120505t190317	723530.199	724742.111	4330476.697	4337402.323	0.627	1.223
G:\gj0512\20120505\NISDVU20120505t191134	723249.560	724504.693	4329653.243	4337105.527	0.711	1.208
G:\gj0512\20120505\NISDVU20120505t192001	719960.620	727563.370	4332813.361	4334063.034	0.631	1.320
G:\gj0512\20120505\NISDVU20120505t193004	712708.970	720155.165	4329034.319	4334376.288	0.510	0.381
summary values (extreme x,y, min ps) :	712708.970	727563.370	4326770.690	4337627.588	0.509	0.381

Step 2: This procedure does a full image ray trace of every image pixel to the DEM surface being used, builds the IGM file that contains the x, y, z coordinates of each pixel center.

- Inputs:
  - mode flag to tell program to ray trace all pixels
  - a flag to indicate if ENVI is available
  - the UTM zone
  - the navout_mout files created in Step 1
  - DEM file
  - Camera file
  - Bin factor in use
- Output:
  - IGM file

Step 3: This procedure uses the IGM file created in Step 2 and a user-supplied slope-aspect file (provided through processing of the LiDAR data) to build the OBS file that lists the ten observation geometry parameters:

1 Path length
2 To-sensor azimuth angle
3 To-sensor zenith angle
4 To-sun azimuth angle
5 To-sun zenith angle
6 Phase
7 Slope
8 Aspect
9 Cosine angle
10 GPS time

- Inputs:
  - Slope_aspect file
  - IGM files
- Output
  - Builds the OBS file

Step 4: This procedure uses the IGM files to create look up table files for each image strip.

- Inputs:
  - Pixel size, rotation (0 for North up), UTM time zone, and the IGM files
- Output:
  - Builds the GLT look-up tables

Step 5: This procedure pushes the designated files through the GLT look-up tables to build orthocorrected images (i.e., fully orthorectified spectrometer data geo-located with the LiDAR discrete point returns). A sample orthorectified spectrometer image for data acquired over Fruita, Colorado during the May 2012 NISDVU flight deployment is shown in Figure 4.

- Inputs:
  - Names of the ortho files to create
  - Names of the GLT file(s) to use
  - Names of the input file(s)
- Outputs:
  - Builds orthocorrect ORT files for one or more input files

6 UNCERTAINTY

The required uncertainty in the Earth location accuracy of the geodesic coordinates computed for individual spatial pixels imaged by the NEON imaging spectrometer is divided into two separate requirements (AD[05]). These are:

AOP-TOR-068 Uncertainty in the knowledge of the position of each spatial pixel on the ground must be less than 0.5 of the imaging spectrometer ground sample distance.

AOP-TOR-069 Uncertainty in the knowledge of the relative position of camera, LiDAR, and spectrometer ground pixels must be less than 0.5 of the imaging spectrometer ground sample distance.

6.1 Analysis of Uncertainty

The accuracy of spectrometer ground pixel locations relate back to the positional and attitude accuracy of the aircraft provided by the onboard GPS and IMU. The initial step in the processing chain is the orthorectification of the discrete LiDAR returns as described in AD[08]. This is a mapping of the discrete LiDAR returns to the Earth surface and generation of a digital elevation model (DEM) from this data onto UTM reference frame. Subsequently, the imaging spectrometer pixels are mapped to the DEM. Therefore, any uncertainty in the Earth location accuracy of geodesic coordinated in the LiDAR-generated DEM will contribute to the uncertainty in imaging spectrometer geolocation estimates. As such, the geolocation error budget has two terms – 1) the geolocation accuracy of the LiDAR processing, and 2) the colocation error between the imaging spectrometer data to the geodesic reference frame defined by the LiDAR DEM.

The uncertainty in the geolocation accuracy of the LiDAR data is determined in the NEON Ll0 to L1 Discrete Return LiDAR processing (AD[08]). In this document, we are considering the co-registration error of the spectrometer pixels to the LiDAR data. In addition, there are additional factors contributing to the uncertainty in co-registration of these data. These manifest themselves as uncertainties in the

spectrometer pixel location on the ground with respect to the digital surface model defined by the LiDAR. Contributors to the uncertainty budget include the boresight error uncertainty between the imaging spectrometer and LiDAR, instabilities in the platform integration mount which result from thermal perturbations during flight and vibration environment, and errors in matching up tie-points during the algorithmic optimization process. These uncertainties are quantified in the following section.

6.2 Reported Uncertainty

The vertical accuracy for the ALTM Gemini LiDAR is provided in the LiDAR Delivery Performance Report (AD[10]). The accuracy is a function of altitude. For a nominal survey flight altitude of 1000 m AGL, the reported LiDAR horizontal accuracy is 1/5500 x altitude, or 0.182 m (1 sigma). Other errors contributing to the LiDAR discrete return geolocation uncertainty are provided in AD[08], and these include uncertainty in lever arm measurement, elevation error, and GPS/IMU orientation and positioning errors.

The total error allocated to the LiDAR geolocation error is 0.2 pixels. This provides a floor for geolocation error attainable for the imaging spectrometer but several additional contributors need to be considered to quantity the error in estimating the uncertainty in estimating the location of ground features as imaged by the imaging spectrometer and by returns from the discrete LiDAR (i.e., the co-registration error).

The errors contributing to the co-registration error between the imaging spectrometer and LiDAR are listed in the following table:

Table 2. Co-registration error budget

Error Source	Budget
Spectrometer boresight error	0.10 pixel
PIM thermal stability	0.10 pixel
PIM mechanical vibration error	0.10 pixel
Error in tie-point optimization	0.15 pixel
Total uncertainty (RSS):	0.23 pixel

Therefore, the uncertainty budget for co-registration between the imaging spectrometer and LiDAR is 0.23 pixel (0.23 m @ 1000 m AGL). The predicted error in geolocation for the imaging spectrometer with respect to the true Earth geodesic coordinates is obtained as the root-sum square of the co-registration uncertainty and the geolocation error:

Table 3. Imaging spectrometer geolocation error

Error Source	Budget
LiDAR geolocation error	0.20 pixel
Spectrometer co-registration error	0.23 pixel
Total uncertainty (RSS):	0.31 pixel

7 VALIDATION AND VERIFICATION

7.1 Algorithm Validation

Validation of the geolocation algorithm consists of two major components: first, the orthorectification of individual pixels with respect to the earth needs to be verified. This is best achieved using accurately geo-referenced ground points distributed across and along a flight line. The error in estimated ground location from the airborne imaging spectrometer data, following application of the geolocation algorithm, can then be estimated.

A series of test flights are planned during the 2014 AOP deployment in Boulder, CO to provide data for data product validation. This involves the accurate measurement of ground control points and the acquisition of imaging spectrometer and LiDAR data at several altitudes over the region. The baseline plan is to measure ground points every 5-meter (or better) along the airport runway used for operations and other nearby buildings to locate corners and edges. These features will then be identified in imagery and optical offsets determined in ground data processing. Absolute horizontal accuracies relative to the ground control points determined using this technique are expected to be better than ±0.05 – 0.08 meter (*Asner et al.*, 2007).

Secondly, the co-registration of the imaging spectrometer data to the LiDAR intensities needs to be determined to validate that the ground features recorded in both data streams have been co-registered to the specified requirements. The different sampling geometries of the LiDAR and spectrometer

combined with aircraft motion and local topography produce additional uncertainty in registering the LiDAR and spectrometer data. The data acquired from the test flights described above can be used for co-registration validation. Data acquired at multiple altitudes will provide a range of collection angles and ground sampling sizes. Registering LiDAR data with spectrometer data is expected to be better than 1/3 pixel (*Asner et al*., 2007). Ultimately, the geolocation accuracy is required to be sub-pixel, our ability to validate this will be limited by the imaging spectrometer spatial sampling. For this reason, a statistical analysis conducted over a number of ground samples may be required to attain the desired validation accuracy.

7.2 Data Product Validation

The algorithm defined in this document produces the orthorectified L1 spectral radiances from raw L0 instrumental data acquired with the imaging spectrometer. The uncertainties in location accuracy of geodesic coordinates computed for individual pixels will be determined experimentally using the calibration procedure described in the previous section. The accuracy is limited by the uncertainty in the aircraft, instrument, and elevation information provided to the algorithm.

8 SCIENTIFIC AND EDUCATIONAL APPLICATIONS

The imaging spectrometer geolocation algorithm provides the intermediate geolocated “at-sensor” radiance product required to produce the orthorectified spectral radiance product. Subsequent processing, including atmospheric correction (RA [04]) are required to produce the L-1 spectral reflectance product as described in RD[05].

It is anticipated that the majority of ecological researchers will utilize the NEON.DOM.SIT.DP1.30006 Spectrometer Surface Directional Reflectance product or higher data products derived from this product in their research. However, it is expected that the geolocated “at-sensor” radiance product will be of interested to some researchers interested in exploratory research or interested in conducting their own atmospheric correction.

9 FUTURE MODIFICATIONS AND PLANS

The imaging spectrometer geolocation algorithm has been fully implemented in research-grade code and operation has been validated using airborne data acquired during the 2012 airborne flight deployments. The current version of the software for this algorithm is written in IDL and requires human interaction at several steps. Future development to be considered may include streamlining, improving, and further automating the code based on operational experience.

10 BIBLIOGRAPHY

Asner, G. P., D. E. Knapp, T. Kennedy-Bowdoin, M. O. Jones, R. E. Martin, J. Boardman, C. B. Field, 2007. Carnegie Airborne Observatory: In-flight fusion of hyperspectral imaging and waveform light detection and ranging (wLiDAR) for three-dimensional studies of ecosystems, Jour. Appl. Remote Sens. (1), 013536 [doi: 10.1117/1.2794018].

Boardman, J. 1999. Precision geocoding of low altitude AVRIS data: Lessons learned in 1998. R. Green (Ed.), 8th Annual JPL Airborne Earth Science Workshop, Pasadena, CA, JPL **99-17**: 63-68.

El-Sheimy, N., 2009. Georeferencing component of LiDAR systems, in *Topographic Laser Ranging and Scanning,* J. Shan and C. K. Toth, Eds., CRC Press, Boca Raton, FL.

Lichti, D., and J. Skaloud, 2010. Registration and calibration, in *Airborne and Terrestrial Laser Scanning*, G. Vosselman and H-G. Mass, Eds., CRC Press, Boca Raton, Fl.

APPENDIX A SCANNING GEOMETRIES OF THE NEON REMOTE SENSING INSTRUMENTS

A.1 Spectrometer Data Acquisition Geometry

The NEON imaging spectrometer (NIS) is a pushbroom spectrometer that provides spectroscopic information at 5 nm continuous samples over the 380 to 2510 nm spectral range with an instantaneous field of view of 1.0 mrad. At a flight altitude of 1500 m, NIS will observe a cross-track swath of 928 m. The IFOV corresponding to a single detector pixel is equivalent to a ground sampling distance (GSD) of 1.5 m at an aircraft altitude of 1500 m (AGL). The concept of a pushbroom imaging spectrometer is illustrated in Figure 10.

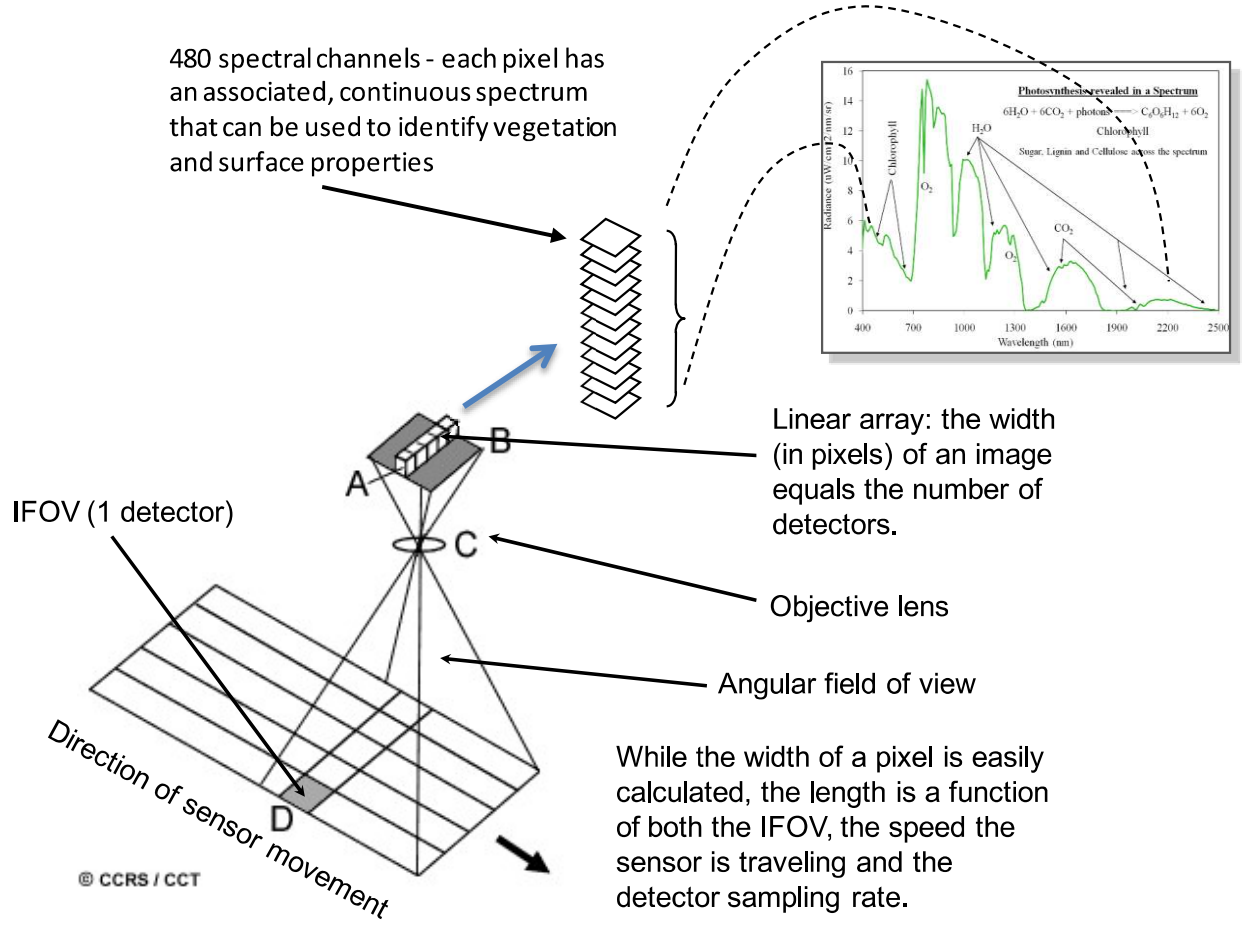

Figure 10. Pushbroom imaging spectrometer concept

The geometry for NIS is shown in Figure 11. The typical flight line is 20 km long and, for a flight altitude of 1500 m, the cross-track swath is 928 m. A single row (line) of 640 cross-track pixels are imaged at a time and data over the full flight line is captured as a result of the forward motion of the aircraft. With an equivalent aircraft ground speed of 50.0 m/sec, 400 seconds or 6.67 minutes are required to scan a single flight line.

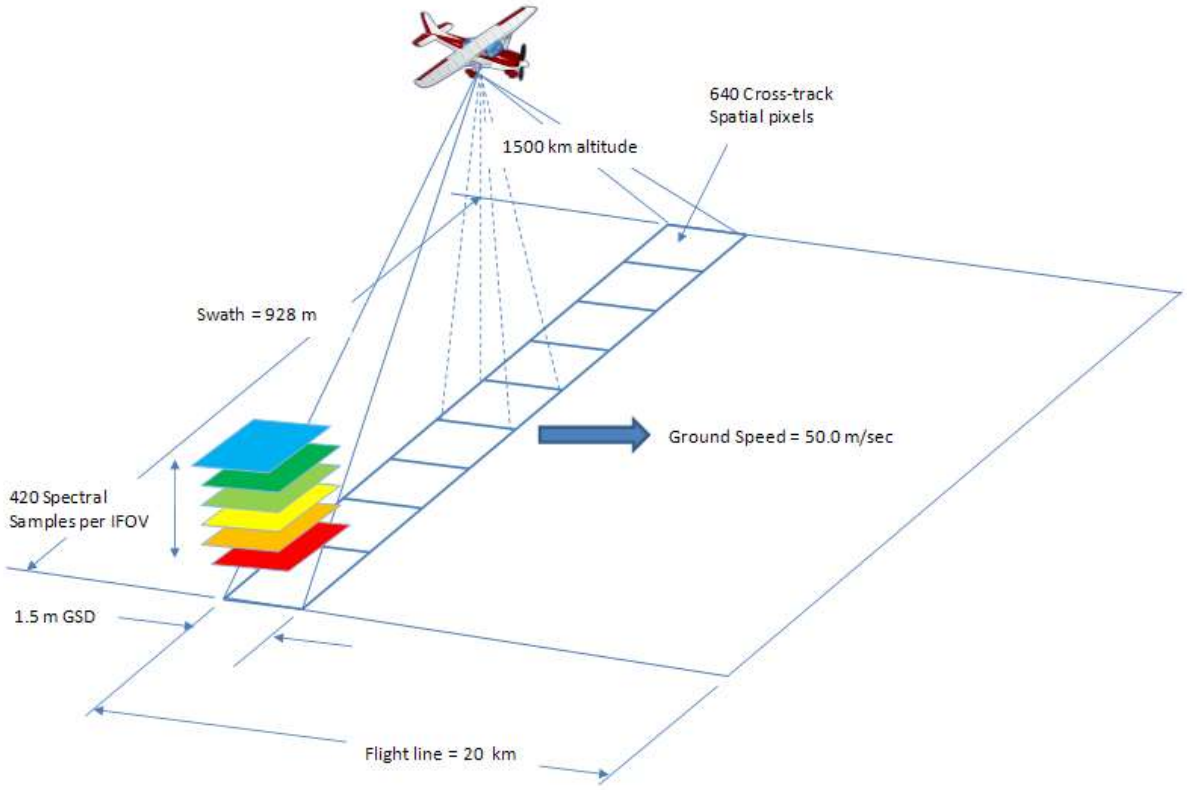

Figure 11. NIS flight geometry

The spectrometer is operated at 100 lines per second, giving a detector integration time of 0.01 sec and resulting in an image smear for a single $IFOV_{along\text{-}track}$ equivalent to (0.01 sec)*(50.0 m/sec), or 0.5 m. Therefore the point spread function in the along-track direction $PSF_{along\text{-}track}$ is smeared over 2.0 m (1.5 m + 0.5 m). The along-track ground sample distance is the distance between two consecutive lines on the ground and is equivalent to (0.01 sec)*(50.0 m/s), or 0.5 m. At 100 lines per second, the spectrometer is oversampling the ground in the along-track direction. The cross-track ground sample distance $GSD_{cross\text{-}track}$ is still related to the IFOV, or 1.5 m. Scene radiance is integrated every 0.01 seconds. For each integration period, data in 640 cross-track pixels is recorded. Associated with each cross-track pixel is a column of 480 spectral pixels, each sampling a 5 nm wavelength interval and in total covering the 380 to 2510 nm spectral range. Not all 480 spectra pixels contain valid spectra information, however all 480 are recorded in the raw data. Thus, for any single integration period, data is recorded in 640 * 480 pixels, or 307,200 pixels total. Each pixel is digitized in a 16-bit word (14 bit dynamic range), resulting in an instantaneous data rate of 4.92×10^6 bits, or 600 Kilobytes. Over a single 20-km flight line, 40,000 along-track lines are acquired, resulting in a total data volume from the NIS instrument of 22.9 GB per flight line. Assuming overlap of 30% between neighboring flight lines, a total of 24 flight lines are required to

survey a single site. Including one minute of calibration data per flight line (3.4 GB), the data volume per site is estimated as 24 * (22.9 + 3.4 GB), or 635 GB.

A.2 LiDAR Data Acquisition Geometry

The NEON AOP incorporates the Optech ALTM Gemini waveform LiDAR. The specifications for this instrument as compared to key AOP requirements are show in Table A1-1.

Table 4. AOP Waveform Altimeter LiDAR requirements compared to the Optech ALTM Gemini Specification

System Parameter	AOP Requirement	Optech ALTM Gemini Specification
Laser wavelength	1064 nm	1064 nm
Laser pulse width	≤ 10 nsec	10 nsec @ 70 kHz
Laser divergence	≤ 1 mrad	User choice (two selections); 0.3 or 0.8 mrad selectable divergence
Pulse repetition frequency	33 to 100 kHz (>150 kHz goal) selectable	33 – 167 kHz (full waveform up to 70 kHz; sub-samples at higher rates)
Waveform sampling	> 8 bits, 1 nanosecond interval	8 or 12 bits, 1 ns interval
Scan frequency	> 50 Hz (selectable)	0 – 70 Hz
Scan angle	≥ 35 degrees	0 – 50 degrees
Elevation error	< 25 cm (1 σ)	< 5 – 30 cm (1 σ)
Horizontal position error	≤ 0.8 m (1 σ)	1/5,500 x altitude (m AGL) (1 σ)
Aircraft altitude	1000 to 3000 meters AGL (1000 meters to 5000 m above sea level)	150 – 4000 m AGL, nominal*
Ground footprint (nadir)	1 to 3 meters (altitude dependent)	Altitude dependent – function of laser divergence

* Operational eye-safe altitudes

The WALi instrument is a cross-track scanning instrument where a scan mechanism serves to direct the transmitted laser beam across the swath as the aircraft moves forward in the along-track direction. As the aircraft moves forward, as series of cross-track scans are built up until a complete flight track is sampled as shown in Figure A-3. Assuming an aircraft altitude of 1500 m, a scan frequency of 40 Hz, and a total mirror scan angle of 40 degrees, the typical cross-track swath (1092 m) is scanned in 12.5

milliseconds. The laser pulse repetition frequency is 70 kHz, so a laser pulse is transmitted every 14.3 microseconds. Therefore, there are 875 shots per swath.

The typical flight line is 20 km in length. At a ground speed of 50.0 m/sec, the flight line is sampled in 400.0 sec (~6.7 minutes). Within this time period, a total of 28.0 x 10^6 shots are sampled (this corresponds to approximately 32,000 cross-track scans). The waveform corresponding to each shot is sampled at 1 nanosecond (ns) intervals. The outgoing pulse is sampled in 40 time bins (1 nsec intervals) and digitized at 12 bits. The return (reflected) pulse is sampled in 440 time bins (also in 1 nsec intervals at 12 bits), resulting in a total of 480 samples per waveform. Therefore, the waveform data volume per flight line is computed as:

$$WALi\ Data\ Volume\ per\ flight\ line = (n_{shots} * n_{samples} * n_{bits})/8 \quad \text{[bytes]}$$

Where,

n_{shots} = number of shots per flight line = 28.0 x 10^6
$n_{samples}$ = number of samples per waveform = 480
n_{bits} = number of bits per sample = 16 (12 bit stored in 16 bit integers)

The right-hand term is the conversion factor from bits to bytes (8 bits per bit). Including discrete returns (in LAS 1.2 format) plus some calibration data (assumed to be equivalent to two extra flight lines per site), the total raw data volume for the WALi per flight is then 3.23 x 10^{10} bytes, or 30.1 GB. This equates to 722.8 GB per site and 2168.3 GB per NEON domain.

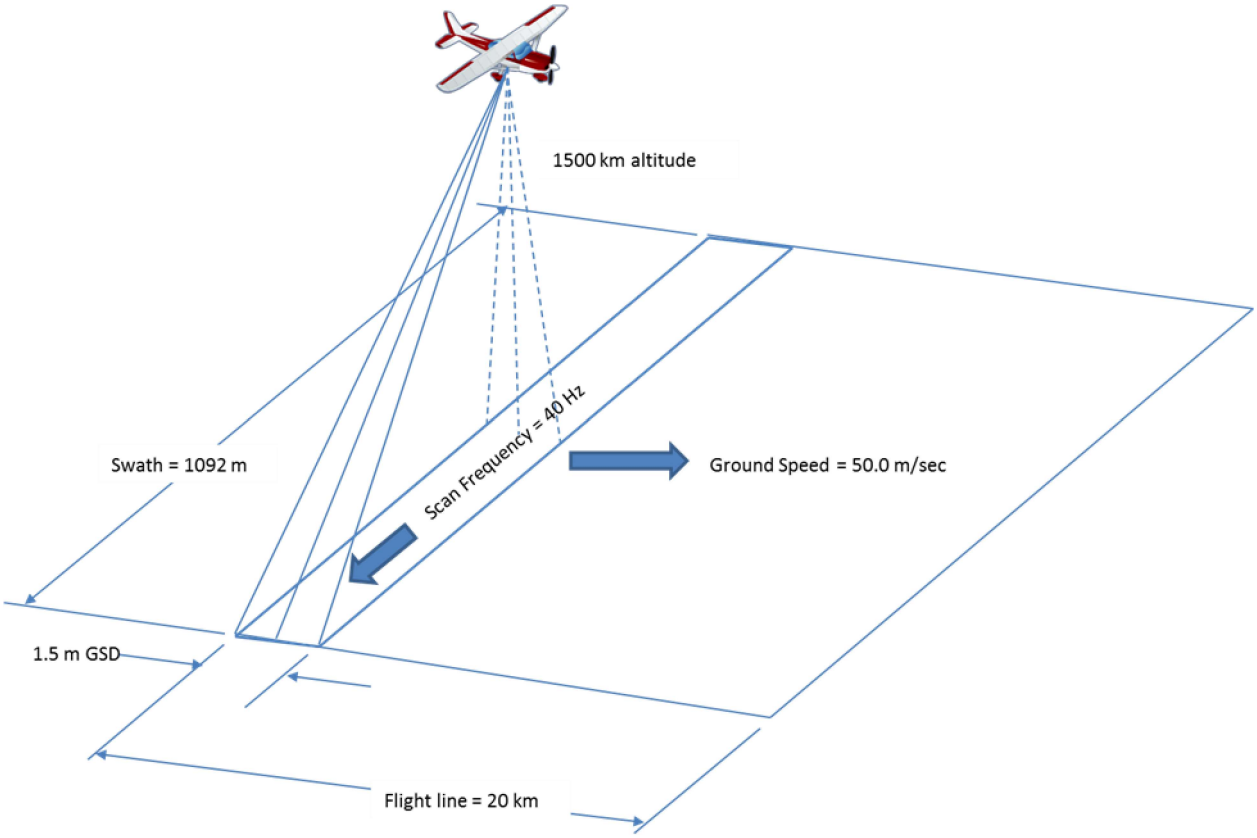

Figure 12. WALi scan geometry

The waveform is obtained by time sampling the laser pulse as it is transmitted from the instrument (out-going) and as it is returned to the instrument after reflection off the vegetation canopy and ground (in-coming or return). The time required for the laser pulse to travel from the aircraft to the ground is

$$t = altitude/c = 1500\ m/2.99x10^{8}\ m/sec\ = 5{,}000\ nsec$$

Therefore, the round-trip time for a pulse of light from the laser to the ground and back is 10,000 nsec. Assuming 440 time bins are allocated to the return waveform, and each bin is sampled in 1 nanosecond intervals, a continuous range of 66 m can be measured:

$$R = R_2 - R_1 = c * \frac{t_2 - t_1}{2} = \left(\frac{2.998x10^{8}m}{\text{sec}}\right) * \frac{(440x10^{-9}sec)}{2} = 66\ m$$

With an outgoing pulse width of 10 nanoseconds, the range resolution (the separation distance required between two objects to distinguish them as two separate objects) is

$$\Delta R = \frac{c * \tau}{2} = \frac{\left(\frac{2.998x10^{8}\text{m}}{\text{sec}}\right) * (10x10^{-9}sec)}{2} = 1.5\ m$$

However, since the return waveform is oversampled at 1 nanosecond bins, using edge detection algorithms surface feature heights can be determined at a range resolution of about 0.15 m. At a pulse

repetition frequency of 70 kHz, the time between pulses is 14,300 nsec which is larger than the two-way travel time for a single pulse of 10,000 nsec. Thus, only a single laser pulse will be in the atmosphere at any given time and there is no ambiguity as to which pulse is sampled on return to the instrument. In some instances it will be desirable to fly at altitudes other than the nominal 1500 m AGL stated, but the important point is that pulse repetition frequency can be tuned to avoid ambiguity over the range of altitudes that AOP will be operating over.

A.3 Camera Data Acquisition Geometry

The digital camera incorporated into the AOP remote sensing payload is the Applanix DSS 449 camera. Specifications for this camera are summarized in Table 5.

Table 5. Applanix DSS 449 camera specifications

Parameter	Value
Image size	5412 (track) x 7216 (x-track) pixels (39 Mpixels)
Pixel pitch	0.0068 mm
Camera focal length	60.0 mm
Field of view	Along-track: 34 deg; useable 31.5 deg Cross-track: 44 deg; useable 39.3 deg
IFOV	0.00011 radians
Shutter speed	125 - 4000 Hz
Dynamic range	12 bits

The camera is operated in step-stare mode as illustrated in Figure A-4. Here we assume an aircraft altitude of 1000 m, and a ground speed of 50.0 m/sec. Initially, an image is acquired at time t_1. At a time t_2, the forward motion of the aircraft causes the camera to image a region some distance D in the along-track direction. Time references are shown at the leading edge of the ground scene in Figure A-4. It is desirable that successive images from the camera capture the ground below in a continuous manner without any gaps. The nominal ground speed of the aircraft is 50.0 m/sec, and for the camera parameters listed in Table A1-2, the along-track image of the detector array is 950 m. Therefore, an image must be acquired every 19.0 sec to obtain gapless imagery. With a camera frame rate of 4000 Hz (i.e., a frame is taken every 0.25 msec), the image smear along track is 0.0125 m. Based on the aircraft altitude and IFOV, the along-track and cross-track GSD at the center of the image (nadir-looking pixel) is 0.17 m.

This situation is somewhat idealized in that it does not account for variation in flight altitude, flight speed, or aircraft orientation which could result in data gaps. To provide margin, we therefore plan to acquire and store frames at shorter time intervals, nominally equal to one-half the time required to traverse the distance equivalent to a full image ($D/2$ in Figure A-4). This is every 9.5 seconds. Thus, every 38,000th frame acquired by the camera is retained as part of the data stream. With a typical flight

line 20 km long (along-track) by 1300 m wide (cross-track), a total of 43 shots/frames are required and the data volume per flight line is calculated as

$$Data\ volume\ per\ flight\ line = (n_{pixels} * n_{bits} * n_{shots})/8 \quad \text{[bytes]}$$

Where:

n_{pixels} = total number of pixels = 3.90×10^7
n_{bits} = number of bits per sample = 16 (12 bits stored in 16 bit integers)
n_{shots} = number of shots per flight line

The result is that the camera data volume is 3.1 GB per flight line, or 75.1 GB per site. The details used in the data volume calculation are provided in Table 6.

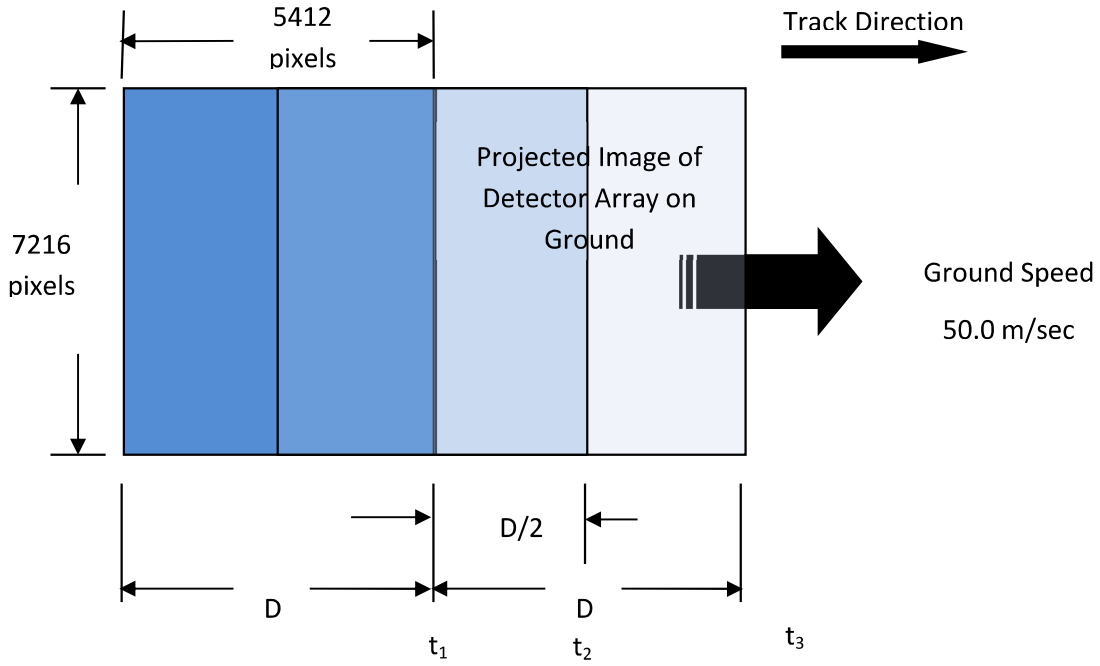

Figure 13. AOP camera scanning approach

Table 6. Typical camera data acquisition parameters

Parameter	Typical Value
Aircraft altitude (AGL)	1000 m
IFOV	0.00011 rad
Geometric GSD_{track} (no smear)	0.11 m
Projected size of detector array on ground	564.0 m (along-track) 714.1 m (cross-track)

Parameter	Typical Value
Aircraft ground speed	50.0 m/sec
Length of flight line	20 km
Number of flight lines per site (30% overlap)	24
Time required to distance D/2, D = 950.0 m	9.5 sec
Number of shots per flight line (10 km)	27
Data volume per flight line	~3.1 GB
Data volume per site	~75.1 GB

APPENDIX B LIST OF FILES

Table 7 contains a list of the different file types used in geolocation process.

Table 7. List of input, intermediate and output files

File type	Description
Input	
camera model	contains the camera parameters:
dem	**d**igital **e**levation **m**odel: elevation of the surface on a regular grid
egm	**e**arth **g**ravitational **m**odel:
sap	**sl**ope and **asp**ect: contains the slope and aspect angles of each pixel in the dem
sbet	**s**moothed **b**est **e**stimate of **t**rajectory: contains the trajectory: location (lat,lon, altitude), attitude (roll, pitch and heading), velocity and acceleration
Intermediate	
eph	ephemeris file: contains
glt	**g**round **l**ookup **t**able: for each raw image pixel, contains the corresponding pixel location in the orthorectified image
igm	contains the x and y locations in UTM of each pixel in a NIS flight line
igm5	as igm, but for only 5 colums in the flight line: the two edges and the 3 central lines
navout_mout	contains x,y,z, roll, pitch, yaw and 3 by 3 attitude rotation matrix for each frame in a flight line
obs	observation file: contains for each raw image pixel: 0: path length 1: sensor azimuth_ 2: sensor zenith 3: sun azimuth 4: sun zenith 5: phase 6: slope 7: aspect 8: cosine of incidence angle 9: gps hour
tim	timing file: contains the gps time for each NIS frame
Output	
rdn_ort	orthorectified radiance
igm_ort	orthorectified igm
obs_ort	orthorectified observation